OPEN ACCESS

KING'S College LONDON

King's Research Portal

DOI:
10.1016/j.colsurfb.2018.09.018

Document Version
Peer reviewed version

Link to publication record in King's Research Portal

Citation for published version (APA):
Harper, R. A., H.Carpenter, G., Proctor, G. B., Harvey, R. D., Gambogi, R. J., Geonnotti, A., ... Jones, S. A. (2018). Diminishing biofilm resistance to antimicrobial nanomaterials through electrolyte screening of electrostatic interactions. *Colloids And Surfaces B-Biointerfaces*. https://doi.org/10.1016/j.colsurfb.2018.09.018

Citing this paper
Please note that where the full-text provided on King's Research Portal is the Author Accepted Manuscript or Post-Print version this may differ from the final Published version. If citing, it is advised that you check and use the publisher's definitive version for pagination, volume/issue, and date of publication details. And where the final published version is provided on the Research Portal, if citing you are again advised to check the publisher's website for any subsequent corrections.

General rights
Copyright and moral rights for the publications made accessible in the Research Portal are retained by the authors and/or other copyright owners and it is a condition of accessing publications that users recognize and abide by the legal requirements associated with these rights.

•Users may download and print one copy of any publication from the Research Portal for the purpose of private study or research.
•You may not further distribute the material or use it for any profit-making activity or commercial gain
•You may freely distribute the URL identifying the publication in the Research Portal

Take down policy
If you believe that this document breaches copyright please contact librarypure@kcl.ac.uk providing details, and we will remove access to the work immediately and investigate your claim.

Download date: 21. Sep. 2020

Accepted Manuscript

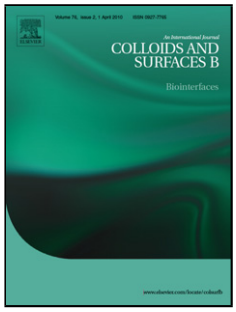

Title: Diminishing biofilm resistance to antimicrobial nanomaterials through electrolyte screening of electrostatic interactions

Authors: Robert A. Harper, Guy H.Carpenter, Gordon B. Proctor, Richard D. Harvey, Robert J. Gambogi, Anthony Geonnotti, Robert Hider, Stuart A. Jones

PII: S0927-7765(18)30629-5
DOI: https://doi.org/10.1016/j.colsurfb.2018.09.018
Reference: COLSUB 9620

To appear in: *Colloids and Surfaces B: Biointerfaces*

Received date: 22-6-2018
Revised date: 30-8-2018
Accepted date: 8-9-2018

Please cite this article as: Harper RA, H.Carpenter G, Proctor GB, Harvey RD, Gambogi RJ, Geonnotti A, Hider R, Jones SA, Diminishing biofilm resistance to antimicrobial nanomaterials through electrolyte screening of electrostatic interactions, *Colloids and Surfaces B: Biointerfaces* (2018), https://doi.org/10.1016/j.colsurfb.2018.09.018

This is a PDF file of an unedited manuscript that has been accepted for publication. As a service to our customers we are providing this early version of the manuscript. The manuscript will undergo copyediting, typesetting, and review of the resulting proof before it is published in its final form. Please note that during the production process errors may be discovered which could affect the content, and all legal disclaimers that apply to the journal pertain.

ACCEPTED MANUSCRIPT

Diminishing biofilm resistance to antimicrobial nanomaterials through electrolyte screening of electrostatic interactions

Robert A. Harper[1], Guy H.Carpenter[2], Gordon B. Proctor[2], Richard D. Harvey[4], Robert J. Gambogi[3], Anthony Geonnotti[3], Robert Hider[1] and Stuart A. Jones[1*]

[1]King's College London, Institute of Pharmaceutical Science, Franklin-Wilkins Building, 150 Stamford Street, London, UK, SE1 9NH.

[2]King's College London Dental institute, Division of Mucosal & Salivary Biology, Tower Wing, Great Maze Pond, London, UK, SE1 9RT.

[3]Johnson and Johnson, Consumer & Personal Products Worldwide Division of Johnson & Johnson Consumer Companies, Inc, 199 Grandview Road, Skillman, NJ, USA, 08558.

[4] Martin-Luther-Universität Halle-Wittenberg, Institute of Pharmacy, Halle (Saale), Germany.

***Corresponding author:** Dr. Stuart A. Jones. King's College London, Institute of Pharmaceutical Science, Franklin-Wilkins Building, 150 Stamford Street, London, SE1 9NH. Tel: +44 (0)207 848 4843. Fax: +44 (0)207 848 4800. E-mail: stuart.jones@kcl.ac.uk

ACCEPTED MANUSCRIPT

ACCEPTED MANUSCRIPT

Graphical Abstract

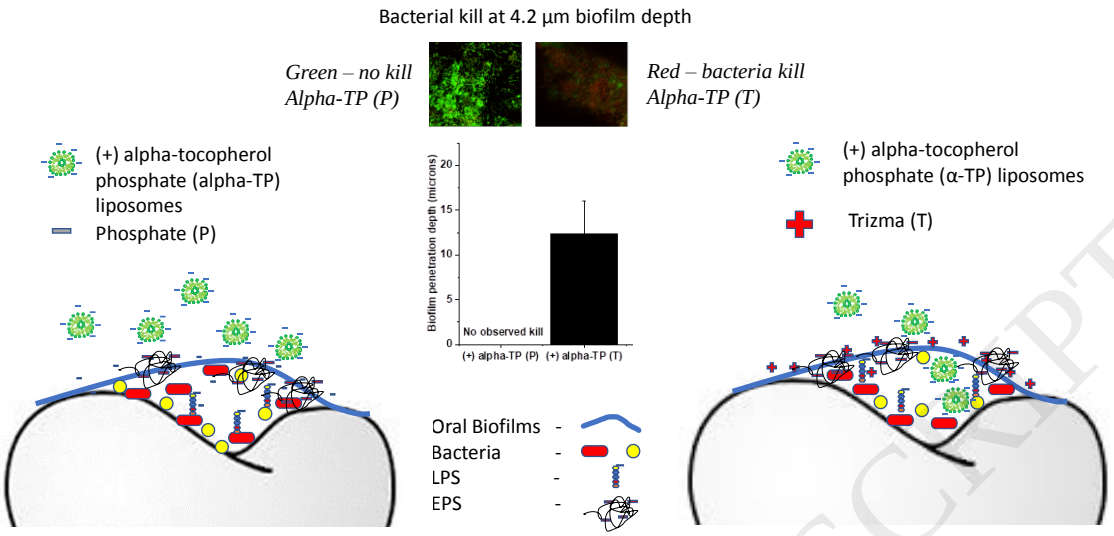

Highlights

- Tris (hydroxymethyl)aminomethane (+ve) electrolytes facilitate the diffusion of anionic alpha-tocopherol phosphate (α-TP) liposomes into multispecies oral biofilms (depth - 12.4 ± 3.6 µm), but phosphate (-ve) electrolytes did not.
- Tris did not modify the surface charge of the α-TP nanomaterials, rather it facilitated the α-TP-biofilm penetration through electrolyte screening.
- The co-administration of cationic electrolytes with anionic nanomaterials is effective in negating the resistance of biofilms to nanomaterial diffusion through charge repulsion.

Abstract

The extracellular polymer substances (EPS) generated by biofilms confers resistance to antimicrobial agents through electrostatic and steric interactions that hinder molecular

ACCEPTED MANUSCRIPT

diffusion. This resistance mechanism is particularly evident for antibacterial nanomaterials, which inherently diffuse more slowly compared to small organic antibacterial agents. The aim of this study was to determine if a biofilm's resistance to antibacterial nanomaterials diffusion could be diminished using electrolytes to screen the EPS's electrostatic interactions. Anionic (+) alpha-tocopherol phosphate (α-TP) liposomes were used as the antimicrobial nanomaterials in the study. They self-assembled into 700 nm structures with a zeta potential of -20 mV that were capable of killing oral bacteria (*S. oralis* growth inhibition time of 3.34 ± 0.52 h). In a phosphate (-ve) buffer the -ve α-TP liposomes did not penetrate multispecies oral biofilms, but in a Tris (hydroxymethyl)aminomethane (+ve) buffer they did (depth - 12.4 ± 3.6 μm). The Tris did not modify the surface charge of the α-TP nanomaterials, rather it facilitated the α-TP-biofilm interactions through electrolyte screening (Langmuir modelled surface pressure increase of 2.7 ± 1.8 mN/ m). This data indicated that EPS resistance was mediated through charge repulsion and that this effect could be diminished through the co-administration of cationic electrolytes.

Key Words: (+) alpha tocopheryl phosphate, antimicrobial, resistance, tooth enamel, nanomaterial, oral biofilm, penetration, electrolyte screening, biological interactions.

Introduction

Bacterial biofilms are structured communities that co-exist within an extracellular matrix [1]. When a biofilm is formed, the bacteria within it become up to 1000 times more resistant to antimicrobial treatment compared to the planktonic organisms [2]. This resistance originates from the creation of subpopulations in the biofilm [3], a higher mutation rate [4], the

ACCEPTED MANUSCRIPT

upregulation of efflux pumps [5], modifications in bacterial lipopolysaccharide (LPS) and a reduction in the diffusion rates of antimicrobial agents in the biofilm matrix, which effectively dilutes the administered agents. These characteristics render it problematic to control biofilm growth once they are established on the surface of materials.

Nanomaterials can physically disrupt biofilms, they can carry antibacterial agents into biofilm communities to control growth [6], [7] and, through modification of their surface chemistry, their interactions with the biofilms can be controlled [8], [9]. Therefore, it has been suggested that nanomaterials can be designed to penetrate and kill bacteria in biofilm communities [10], [11]. However, because each biofilm can show significant variability with respect to the organisms and extracellular components that it contains [12] and nanomaterial diffusion is inherently slower than small organic antimicrobials, designing a nanomaterial that has the surface properties to allow it to efficiently diffuse into a multispecies biofilm after deposition onto a material surface is not a trivial task [13], [14], [15]

One approach that could reduce the biofilm resistance to nanomaterial diffusion is to co-administrator a penetration enhancer in order to modify the biofilm interactions with the nanomaterial surfaces. In a similar manner to other biological barriers, e.g., epithelial mucus, bacterial biofilms restrict the diffusion of xenobiotics, within their structured communities, through steric hindrance and electrostatic interactions [16]. The electrostatic interactions in biofilms arise from the outer surface of the bacteria, which are generally negatively charged due to their lipoteichoic acid and lipopolysaccharide components, and the extracellular polymer substances (EPS) [17], which can also be negatively charged. Therefore, it seems feasible that cationic penetration enhancers could be useful to screen biofilm electrostatic interactions in attempt to dampen their capability to resist nanomaterial diffusion.

Biofilm electrostatic interactions with antimicrobial nanomaterials could be screened using electrolytes because as electrolyte concentration increases in the biofilm it would be

ACCEPTED MANUSCRIPT

expected that there would be a reduction of the Debye length of the functional groups on the EPS [18]. For example, at an ionic strength of 0.1 mM, the charge effect, *i.e.*, Debye length, should extend by approximately 10 nm, while at 100 mM, it should only extend about 1 nm from the surface of the EPS. This would increase the effective pore size by about 10 nm as the ionic strength is increased from 0.1 to 100 mM, which could have a significant effect on the diffusion of nanomaterials through oral biofilms [19]. Previous work has suggested that electrolyte screening interactions do not influence the diffusion of small nanomaterials encountered during environmental exposure, but there is emerging evidence that it could be significant for larger nanomaterials, *i.e.*, those used to deliver antimicrobial agents as they are typically larger than 10 nm [16], [20].

Understanding the screening potential of electrolytes in biofilms could also provide valuable information about the properties of the biofilm EPS. Although it has been stated that the EPS is negatively charged in biofilms it is known that the EPS produced by different species of bacterial varies greatly in composition [21]. These variations generate regions in the EPS that have a different electrostatic charges and different steric interactions due to changes in the component's molecular weight (0.5-2.0 x 10^6 Da) [22]. Studies have confirmed that EPS composition changes influence biofilm interactions with lectins, lipids and the surface of bacteria, but very little work has been performed to understand how the EPS composition influences the access of antimicrobial nanomaterials to the bacteria within the biofilm [23]. One of the reasons is that when fully hydrated, the bulk properties of biofilms can be very similar to those of water, making it difficult to delineate the barrier between the biofilm and the surrounding bulk liquid [24].

The aim of this study was to investigate if the resistance of biofilms to the penetration of antimicrobial nanomaterials could be overcome through the co-administration of electrolytes that screen the biofilms electrostatic interactions with the result of enhancing the

ACCEPTED MANUSCRIPT

nanomaterial's antimicrobial action. The mono alkyl phosphate amphiphile vitamin (+) alpha-tocopherol phosphate (α-TP) was selected as the test antimicrobial agent. Phosphate amphiphiles can form a range of different types of nanomaterials and they are arguably one of the most flexible types of anti-biofilm systems. They can act directly to disrupt bacterial biofilms or they can be loaded with an antimicrobial agent, which they can deliver into biofilms [25], [26]. α-TP was specifically selected in this study as it has been shown to form bi-layer islands in aqueous vehicles with a negative surface charge, thus if presented to a biofilm with a negatively charged EPS, electrolyte screening could potentially increase the penetration of these nanomaterials into the biofilm [27]. The naturally occurring α-TP stereoisomer (RRR, + or d) was employed in the study as it has been previously shown to have direct antimicrobial activity, but as it was not easy to extract from natural sources it synthesised from (+) alpha tocopherol (α-T) [18]. An oral multispecies biofilm was used in the study because previous work had suggested that oral biofilms display a net negative charge [19] and thus they would restrict the diffusion of the α-TP into the biofilm by electrostatic repulsion. In addition, it was perceivable that the phosphate nanomaterials and electrolytes could be co-localised for an extended period of time in oral biofilms *in-vivo*, thus the study results may be of practical significance in the field of oral hygiene [28]. In-keeping with the potential practical use of the study data the test agents were always dissolved in a 20% ethanol 80% water vehicle at pH 7.4 as it mimicked an oral healthcare product. The negatively charged phosphate, predicted to have very little effect on the nanomaterial-biofilm interaction, and the positively charged Tris ((hydroxymethyl)aminomethane), predicted to screen the biofilm-nanomaterial interactions through its three ethyl alcohol groups, were used in the study as both these electrolytes are known to be capable of adsorbing at biological interfaces [29]. As the addition of the electrolytes to the biofilm system also had the potential to modify the antimicrobial nanomaterial size, surface polarity and charge these

ACCEPTED MANUSCRIPT

characteristics were assessed using light scattering and fluorescence spectroscopy. Confocal microscopy was used to investigate the multispecies salivary biofilm penetration of the aggregates in the presence of the two different electrolytes [30]. These penetration results were investigated in more detail by studying the effects of the electrolytes on the interactions of the nanomaterials with artificial Gram-positive bacteria membranes, using a Langmuir trough, and the effects of the electrolyte nanomaterial combinations on the bacteria growth inhibition using a single species of oral bacteria, *Streptococcus oralis*, a primary coloniser in the mouth [31].

Experimental Section

Materials

(+) α-T (Type VI, ~ 40% purity), phosphorus oxychloride ($POCl_3$) (≥ 99%), tetrahydrofuran (THF) (anhydrous) (≥ 99.9%), trimethylamine (≥ 99%), trifluoroacetic acid (≥ 99%), Tris hydrochloride (≥ 99%), cetylpyridinium chloride (CPC) (99.0-102%), brain heart infusion (BHI) broth and glycerol were purchased from Sigma Aldrich, UK. Absolute ethanol, propan-2-ol, hexane fractions (60-80), disodium hydrogen phosphate, monosodium dihydrogen phosphate, blood agar (BA) plates containing blood agar base no. 2 with 5 % horse blood, 0.2 μM nylon syringe filters, hydrochloric acid and sodium hydroxide were purchased from Fisher scientific Ltd, UK. De-ionised water was used from laboratory supply. Hydroxyapatite discs (5 mm diameter x 2 mm thick) were purchased from Himed inc, USA. Live/ dead ® BacLight™ bacterial viability kit, for microscopy, was purchased from Life Technologies, UK. *S. oralis* NCTC 7864T was purchased from LGC standards, USA. 1-palmitoyl-2-oleoyl-sn-3-glycerophospho-1-glycerol (POPG) and 1-palmitoyl-2-oleoyl-sn-3-glycerophosphocholin (POPC) were purchased from Avanti polar lipids, USA. Chromatographic paper, 10 mm x 100 m was purchased Whatman, Maidstone, UK. Plastic

ACCEPTED MANUSCRIPT

syringes (1 and 20 mL) were purchased from Terumo, Philippines. Syringe needles were purchased from Macrolance, Ireland. Disposable clear dynamic light scattering cuvettes (macro, PMMA) and disposable folded capillary cells (DTS1070) where purchased from VWR, Germany. Clear sterile polyester adhesive films were purchased from Starlab, UK.

Methods

(+) α-TP Synthesis

(+) α-TP was synthesised as previously described to generate a natural, non-commercially available isoform [18]. In brief, (+) α-T was phosphorylated in the presence of phosphorus oxychloride with triethylamine in anhydrous THF for 3 hours at room temperature. The triethylamine hydrochloric acid salt was removed and the solution was hydrolysed in water for 24 hours. (+) α-TP was then extracted into hexane, into water at basic pH and again into hexane at acidic pH to remove the impurities. The product was purified by C18 chromatography.

(+) α-TP aggregate characterisation

To understand the effects of the electrolytes on the self-assembly of (+) α-TP, fluorescence emission spectra of (+) α-TP (195 µM) dispersions were recorded using a fluorescence spectrometer fitted with a Xenon pulse lamp (Varian Cary Eclipse Fluorescence Spectrometer, Agilent Technologies, UK). A fluorescence cell (Helima fluorescence cell 10mm, Helima UK Ltd., UK) with a 10 mm path length was used. Excitation and emission slits were fixed at 5 nm. In all measurements, the excitation wavelength was set at 286 nm. The samples were scanned from 250 to 450 nm at a wavelength scan rate of 120 nm/ min with a PMT detector gain of 600 V. The experiments were performed at a temperature of 25 °C. Fluorescence emission intensity increases/ decreases at 310 nm were monitored and

ACCEPTED MANUSCRIPT

normalised as shown in equation 1. The normalised data points were then plotted against ion concentration (Tris or phosphate). Analysis of the spectra was conducted using OriginPro software (OriginPro version 2016, OriginLab Corporation, US) and the dose dependent analysis selected to assess trend patterns.

$$F_n(\%) = \frac{F_s - F_{min}}{F_{max} - F_{min}} X100 \qquad \textit{[Equation 1]}$$

Where F_n is the percentage normalised fluorescence, F_s is the sample fluorescence, F_{min} is the minimum fluorescence and F_{max} is the maximum fluorescence. The size of the aggregates (100 µM, n = 3) were analysed by photon correlation spectroscopy (Malvern Nanoseries Zetasizer, Malvern Instruments Ltd, UK). Detection of the light scattering signal was performed at 173 ° at 25 °C. The material refractive index was set at 1.59, the material absorbance at 0.01, the dispersant refractive index at 1.3469 and the sample viscosity (cP) at 2.143. Blank solutions (containing just solvent) were used as a control. The same instrument measured the zeta potentials using a dielectric constant of 78.5 and Smoluchowski (1.5) interpretation of the data with (+) α-T in Tris buffer (25mM) as a control. The chemical stability of the (+) α-TP was measured as described previously [18].

Bacterial model membrane interactions

A Langmuir trough (Nima technology equipment, Coventry, UK) with a circular PFA trough (5 cm^2, volume 20 ml) on a stir plate (Whatman stirrer, WC-303) with subphases of either a Tris or phosphate buffer (10 mM, pH 7.4) were employed. The phospholipids used to represent the lipid component of the bacterial plasma membrane were anionic POPG and zwitterionic POPC as they have been previously used in monolayer experiments as bacterial membrane mimics [32]. Although a large component of plasma membranes is made up of proteins and indeed (+) α-TP has been found to be internalised *via* protein channels [33], they

ACCEPTED MANUSCRIPT

were not included in this model as the anionic (+) α-TP is likely to require an initial attraction through the cationic components of the plasma membrane (lipidic and protein components), *i.e.* cationic choline components, before internalisation in oral bacteria and our aim is to assess how cationic and anionic buffer effects manipulate this electrostatic attraction. To understand the effects of the electrolytes on the membrane architecture, POPC: POPG (3:1 mg/ ml, dissolved in chloroform) (lipid ratio was optimised in preliminary experiments) lipids were deposited drop-wise at the air/ liquid interface until their maximum surface pressures were achieved. To assess the nanomaterial-membrane interactions, the lipids were again deposited drop-wise at the air/ liquid interface until a 30 mN/ m pressure was reached in the Tris buffer subphase (as this is the pressure of a bacterial membrane [34]) or the maximum pressure that could be achieved for the phosphate buffer subphase (always > 30 mN/m). The lipid monolayer was allowed to equilibrate over 30 min at room temperature to allow a stable surface pressure to be obtained (drift in surface pressure, ≤ 0.2 mN/ m over 2 minutes using Nima TR516 software). The α-TP samples (0.1 mL, 3 mM, in 20% ethanol, 80% water, 150 mM phosphate or Tris at pH 7.4) were injected into the subphase with surface pressure monitored over time at a constant surface area. Experiments were repeated in triplicate. Vehicle injections of 0.1 mL, 20% ethanol, 80% water (150 mM Tris , pH 7.4) were also conducted and any induced pressure changes were recorded as controls.

S. oralis **growth retardation**

The assay was performed to assess if the electrolytes influenced (+) α-TP's antimicrobial activity in inhibiting streptococci biofilm growth. *S. oralis* NCTC 7864T, stored in brain heart infusion (BHI) broth with 10% glycerol at -70°C, was cultivated on blood agar (BA) plates containing blood agar base no. 2 and 5 % horse blood, at 37°C under aerobic conditions for *S. oralis*. Plates were subcultured every 48 h and passaged no more

ACCEPTED MANUSCRIPT

than 6 times. Aliquots of BHI broth (20 mL) were inoculated with 3-4 colonies of bacteria from plates that had been growing the bacteria for 24 h. After 18 h of growth 20 µl of bacteria were then inoculated in a new BHI broth (20 mL, 37 °C). When an optical density reading between 0.2-0.3 (200 µL) was obtained at 620 nm (ABS_{620}) (*i.e.* the bacteria were in their exponential growth phase) the bacterial cells were washed twice by centrifugation (1614 g, 10 min, 25°C) with sterile saline (20 mL), and re-suspended in saline to provide an ABS_{620} reading of 0.16 (UV-Vis plate reader, iEMS Incubator/ Shaker, Thermo Scientific,UK). Aliquots (200 µL) of the cell suspension were transferred to the wells of a sterile 96-well microtitre plate. The plate was sealed and centrifuged for 60 min at 2046 g. The supernatant was removed by inverting the plate leaving an *S. oralis* biofilm at the base of each well. The wells were treated in triplicate with one of the three α-TP aggregate formulations (200 µL) for 2 min. The test solutions were removed and the cells washed with saline (200 µL) twice. Aliquots (200 µL) of BHI were added to the wells. The plates were sealed with clear sterile polyester adhesive films and incubated in aerobic conditions at 37°C in the UV-Vis plate reader for 24 hours, taking 620 nm absorbance readings every 15 minutes. The Richards model (Equation 2) was used to describe the growth curves [35].

$$ABS_t = ABS_{min} + \frac{ABS_{max} - ABS_{min}}{[1 + exp\,(-\mu ABS^{*} m^{*}(t - t_i)]^{1/m}} \qquad \textit{[Equation 2]}$$

Where ABS_t was the absorbance at time, ABS_{min} and ABS_{max}, represent the asymptotic minimum and maximum absorbance's, µABS was the maximum specific growth rate, t was the time (h), t_i was the time to inflection (measure of lag time), or time to the point at which the sign of the curve changes from a positive curvature to a negative curvature or vice versa, and m was the modifier for growth dampening. The growth curve data were entered into the Originpro 2016 software programme (OriginLab Corp., USA) and a nonlinear curve fit was performed on each growth curve to determine t_i and ABS_{max} for each

ACCEPTED MANUSCRIPT

treatment run. The t_i value indicated the growth time to inflection points and ABS_{max} measured the post-growth maximum population densities. Each experiment was performed on three separate occasions.

Biofilm penetration

The penetration assay investigation whether the electrolytes influenced (+) α-TP's ability to penetrate into multispecies oral biofilms. One hydroxyapatite (HA) disc was added vertically to a micro centrifuge tube containing UWMS (one donor, 400 µL) and incubated at 37 °C for 18 h. After their 18 h of incubation in unsterilised UWMS the HA discs were removed, added to a fresh aliquot of sterilised heat-treated (10 min, 80 °C) UWMS (200 µL) incubated at 37 °C for 24 h, removed, washed with saline (600 µL) and treated with Live/ dead BacLight bacterial viability kits. Biofilms were observed using 63x oil immersion objective and a Leica sp2 confocal microscope with 488 and 568 nm excitation and 500-530 nm (green fluorescence representing up take of Syto 9 by live cells) and > 620 nm (Red fluorescence representing up take of propidium iodide by dead cells) emission filters. Images were taken near the centre of the HA discs both sides. There was no cross over between emission spectra and excitation intensities were ≤ 31%. The biofilm growth was considered normal if they grew 30 – 60 µM. Biofilm red / green ratios as a function of biofilm depth were measured using the z-stacking tool at 63x magnification taking an image every ~1 µm. The HA discs were then completely submerged in one of the three different α-TP aggregate test solutions (200 µL) in new micro centrifuge tubes for 2 minutes before being washed with saline (600 µL). HA discs were then re-exposed to live/ dead staining for 1 h and imaged again. Changes in the ratios of the red/ green staining as a function of biofilm depth demonstrated each of the three samples biofilm kill penetration. These studies were repeated in triplicate for each test solution. CPC was used as a positive control. Each HA disc was

ACCEPTED MANUSCRIPT

imaged on both treated sides in two different areas near the centre of the discs. As a sterility control, sterile saliva was incubated with a sterile HA disc and showed no biofilm growth. In some cases, discs were only imaged once, after biofilm test sample exposure, to ensure kill was caused by antimicrobial activity and not by the dual imaging and staining process.

Statistical analysis

All data were expressed as their mean ± standard deviation (SD). Statistical analysis of data was performed using Levine's homogeneity test and ensured all sample group data was of acceptable distribution ($P > 0.05$) before statistical significance between the sample groups was assessed by one way analysis of variance (ANOVA) tests with post-hoc Tukey analysis in Origin 2016. Statistically significant differences were assumed when $p \leq 0.05$.

Results

(+) α-TP aggregate characterisation

The increase in the attenuated derived count rate compared to the vehicles (149 ± 59.4 kcps, $p < 0.05$) confirmed the (+) α-TP (100 μM) was forming aggregates in the 20% ethanol 80% solvent systems at pH 7.4 utilised in this work. At low electrolyte concentrations (< 1 mM) increasing concentrations of Tris in the (+) α-TP vehicle increased the fluorescence emission intensity from the aggregates, the converse was true when (+) α-TP was dispersed in a phosphate buffer solution (See supplementary material, Figure S1).

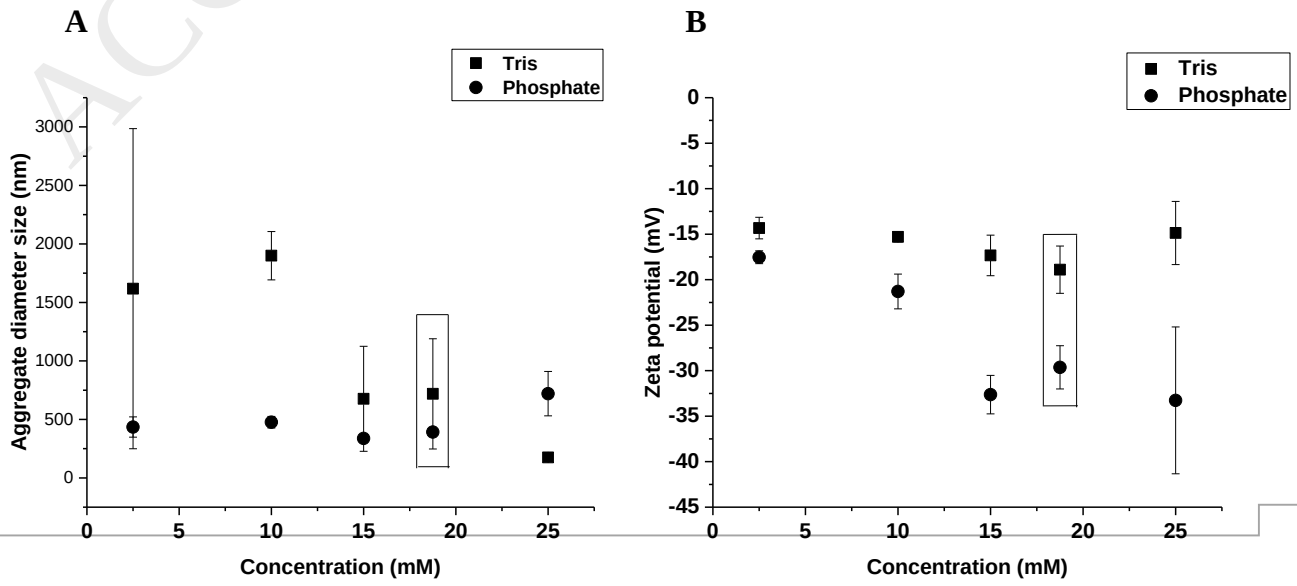

ACCEPTED MANUSCRIPT

Figure 1: *Effect of buffer on aggregate architecture. Comparison of (+) α-tocopheryl phosphate (0.1mM) aggregate size (A) and zeta potential (B) when formulated with increasing concentrations of Tris (Tris) or phosphate at pH 7.4 in 20% ethanol 80% water vehicles. Data represents mean ± SD, n=3. Aggregate: ion ratio of 1:187.5 highlighted by a box).*

At electrolyte concentrations (between 1 mM and 25 mM) addition of phosphate was not shown to have a significant effect on the (+) α-TP aggregate size, but addition of Tris did reduce (+) α-TP size and size distribution, although there was not a clear concentration dependant effect of Tris on aggregate size (Figure 1A). The (+) α-TP aggregates in the presence of Tris were found to consistently have a lower negative zeta potential than when in the presence of phosphate ($p < 0.05$), but this zeta potential did not change significantly with increasing levels of electrolytes. The phosphate electrolyte gave a concentration dependent increase in negative surface aggregate charge (Figure 1B). In light of the fact that the size of aggregates have previously been shown to be influential in the biofilm penetration of phosphate amphiphile aggregates [27], the size and zeta potential data resulted in a fixed (+) α-TP: ion ratio being used (1:187.5) in the subsequent biofilm studies order to maintain a similar aggregate size ($p > 0.05$) in the presence of the two different electrolytes such that electrostatic interactions screening could be evaluated without major confounding effects.

Bacterial model membrane interactions

The POPC: POPG (3:1) phospholipids were capable of reaching a maximum surface pressure of 38 ± 1.5 mN / m when deposited on the Tris buffer subphase, but they were only

ACCEPTED MANUSCRIPT

capable of reaching a maximum surface pressure of 15.2 ± 8.5 mN / m when deposited on the phosphate buffer subphase (Figure 2A). This demonstrated that the cationic Tris and anionic phosphate buffers interacted with the ionic phospholipids and modified the monolayer architecture with Tris allowing more effective membrane packing compared to the phosphate electrolytes.

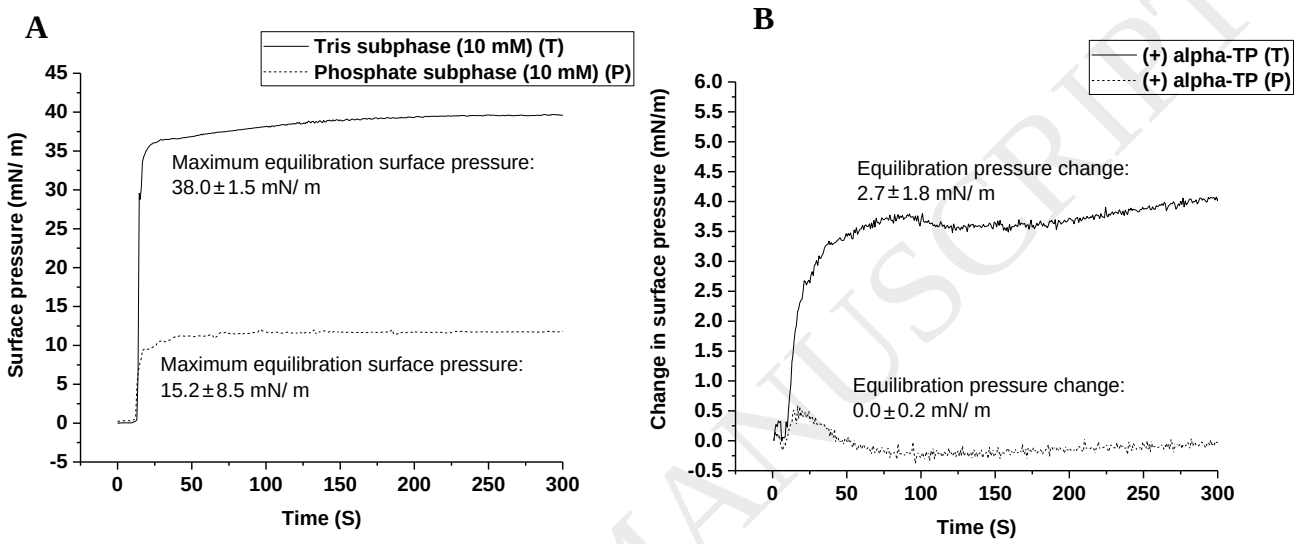

Figure 2: *Effect of electrolytes on bacterial monolayer (POPC: POPG (3:1)) architecture and nanomaterial interaction. (A) Maximum constant area monolayer surface pressure achieved using a Tris (T) or phosphate (P) subphase (B) Monolayer surface pressure change due to (+) alpha tocopheryl phosphate nanostructures injection into the subphase.*

When the (+) α-TP aggregates were co-administered with Tris to the Langmuir subphase, the monolayer equilibration pressure (set at 30 mN/ m to replicate the pressure of bacterial membranes) was found to immediately increase by 2.7 ± 1.8 ($P > 0.05$) showing a favourable interaction of (+) α-TP with the monolayer (Figure 2 B). When (+) the α-TP was co-administered with phosphate into the Langmuir subphase, there was no increase in monolayer pressure indicating a negligible interaction of (+) α-TP with the monolayer. The vehicle alone was found to slightly reduce the surface pressure over time (1 mN/ m over 5

ACCEPTED MANUSCRIPT

min), presumably due to the ethanol-induced phase transition effect of ethanol on the POPC: POPG monolayer in the application vehicle, but this was not thought to be consequential in the experiments reported herein (See supplementary data, Figure S2) [36].

S. oralis biofilm growth inhibition

The (+) α-TP co-administered with Tris displayed a significant retardation of bacteria growth (inflection point 3.34 ± 0.52 h) compared to a Tris vehicle alone (1.69 ± 0.17 h, $p = 0.0001$) (Figure 3 A). The (+) α-TP nanostructures co-administered with phosphate electrolytes had no significant effect on bacterial growth (2.01 ± 0.30 h, vs vehicle of 1.81 ± 0.15, $p > 0.05$). Interestingly both the (+) α-TP systems reduced the post-growth maximum population density of S. oralis ($p < 0.05$ compared with vehicle controls) (Figure 3 B). Thus, it appeared that the Tris facilitated decreased growth effect on S. oralis (since time to inflection point was increased) whereas the phosphate caused increased death rate shown in the maximum population density, i.e., when the growth rate equals the death rate.

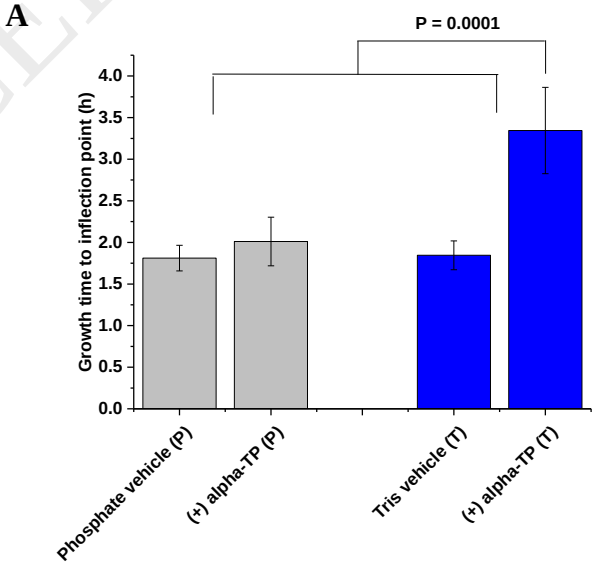

ACCEPTED MANUSCRIPT

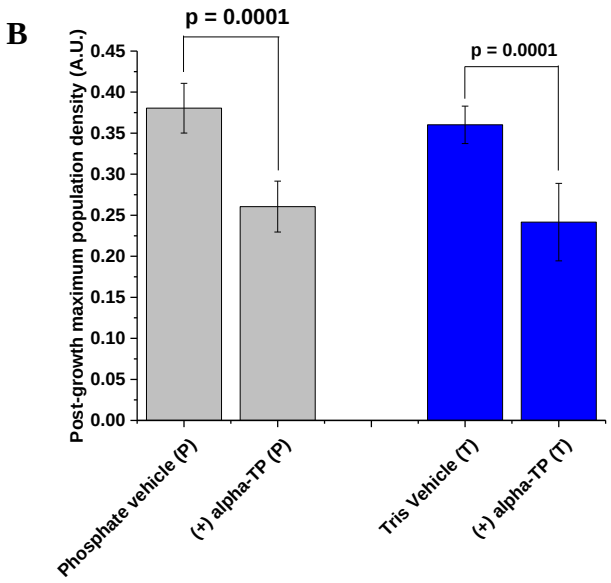

Figure 3: *Effect of electrolytes Tris (T) and phosphate (P) on (+) alpha tocopheryl phosphate nanostructure (A) inhibition of Streptococcus oralis growth and* (B) *inhibition of Streptococcus oralis population density. Data shows mean ± standard deviation, n=3.*

UWMS biofilm kill penetration

The confocal images of (+) α-TP aggregates co-administered with Tris (-18.9 ± 2.6 mV zeta potential, 718 ± 471 nm diameter) showed an effective kill of the bacteria at a biofilm depth of 4.2 um, but they had no kill at 15 microns (see supplementary material, Figure S4). The Tris vehicle alone was found not to kill any bacteria in the salivary biofilms (see supplementary material, Figure S5). The biofilm kill penetration depths were considered to be at the points where post (+) α-TP application live/ dead staining ratios matched that of the pre (+) α-TP application live/ dead staining ratios, *i.e.*, there was no longer any sign of bacterial kill (see supplementary material, Figure S3) . The bactericidal penetration depth of the (+) α-TP aggregates dispersed in Tris was calculated as 12.4 ± 3.6 um. CPC, which acted as a positive control, killed bacteria in the biofilm to a depth of 16.1 ± 4.3 microns. The (+) α-

ACCEPTED MANUSCRIPT

TP co-administered with phosphate (-29.6 ± 2.4 mV zeta potential, 392 ± 6 nm diameter) was not capable of killing bacteria in the biofilms (Figure 5).

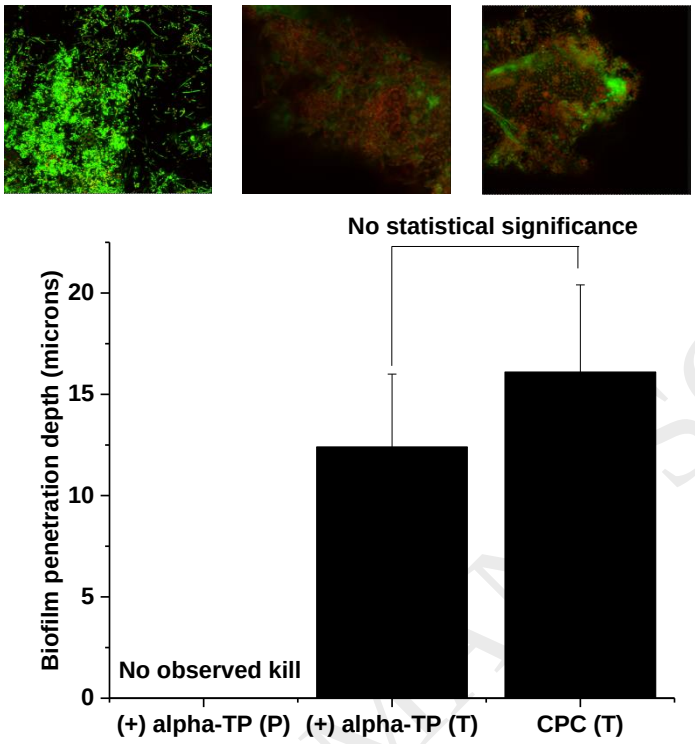

Figure 5: *Effect of electrolytes on unsterilized whole mouth saliva biofilm kill penetration depths of (+) alpha tocopheryl phosphate. Top, live/ dead stain confocal microscopy images at 4.2 micron depths. Bottom. Biofilm penetration depths of +) alpha tocopheryl phosphate with Trima (T) and phosphate (P) compared with cetylpyridinium chloride (CPC) in Tris as a positive control. N=3 results bars show mean ± standard deviation.*

Discussion

The phosphorylation of (+) α-T generated (+) α-TP, which displayed a negatively charged phosphate head group at physiological pH. The dynamic light scattering data for (+) α-TP confirmed that it formed aggregates at the nanoscale in a polar disperse phase that mimicked a mouthwash solution. The type of aggregates that (+) α-TP formed in the presence

ACCEPTED MANUSCRIPT

of Tris have previously been reported to be planar bilayer islands [18]. Attempts in this work to characterise the aggregate type in the phosphate buffer failed because, unlike the Tris system, the precipitation of the phosphate salt upon sample preparation made it impossible to obtain reliable atomic force microscopy images. However, the fluorescence and light scattering measurements did provide information on the effects of the Tris and phosphate electrolytes on the properties of the (+) α-TP aggregates. The increase in fluorescence intensity upon the titration of low concentrations of Tris into the disperse phase of the (+) α-TP suggested that aggregate surface potential decreased upon the addition of Tris [37] and this translated into a lower zeta potential of the aggregates in Tris compared to the phosphate buffer. Increasing the concentration of Tris in the (+) α-TP system also reduced the size and size distribution of the (+) α-TP aggregates. However, at higher Tris concentrations no concentration dependent effects on aggregate zeta potential were observed. This data suggested that Tis influenced the corona surrounding the phosphate amphiphile polar head group to decrease the water organisation at the membrane interface and supress the surface charge [34], but it was not capable of neutralising the molecular charge and hence the Tris interactions were not thought to be very strong. Likewise the phosphate showed, through both the fluorescence and zeta potential measurements that the electrolyte was associating to some degree with the (+) α-TP aggregates and enhancing the negative charge of the aggregates. The strengthening of the aggregate surface charge could have been a consequence of the negative inorganic phosphate groups (HPO_4^{2-}/ H_2PO^-) associating with the (+) α-TP aggregates surfaces ($R\text{-}OPO_3H^-$/ $R\text{-}OPO_3^{2-}$) through hydrogen bonding, hence its greater effect on aggregate zeta potential compared to the Tris . It is known that electrolytes such as Tris, carbonate, cacodylate, phosphate and citrate do not only set the bulk solvent pH, they also adsorb to the interfaces to affect the nanostructure dispersion and electrophoretic mobility [38]. It appeared in this study that, for phosphate this resulted in surface charge amplification as a result of adsorption of

ACCEPTED MANUSCRIPT

like-charged ions (co ions) onto the charged aggregate surfaces [39], whilst for Tris aggregate absorption resulted in a mild suppression of the zeta potential. The characterisation of the (+) α-TP aggregates in the two electrolyte solutions allowed the selection of two materials with a similar size, identical electrolyte concentration, but different surface charges to use in the subsequent biofilm experiments.

The Langmuir experiments showed that the electrolytes, in the absence of the (+) α-TP aggregates, had an effect on the monolayer in a similar manner to previously published studies [40], [41]. POPC is a zwitterion, whilst POPG is anionic hence together the POPC: POPG (3:1) monolayers display a net negative charge, resulting in electrostatic attraction between cations such as Tris with the anionic POPG head groups. This ion-pairing can swell the phospholipid supramolecular structures and create 'gaps' in the monolayer, which are filled by additional phospholipids that increase the surface pressure compared to the monolayer formed without the cationic electrolytes [42]. The phosphate electrolytes also interacted with the deposited POPC: POPG phospholipids, probably though ion-pairing with choline and hydrogen bonding with the organic phosphate groups in a similar way to the interactions observed on the (+) α-TP nanostructure surfaces (enhanced negative zeta potential) [43], [44] The increase in monolayer electronegativity with the phosphate electrolytes was observed as they were less effective in encouraging additional phosphates to pack into the monolayer and hence it achieved a lower surface pressure compared to the Tris system. [45], [46], [47], [48], [49], [50], [51]

Setting the equilibration pressure of the model bacterial monolayer to 30 mN/ m (equivalent to that of bacteria) and monitoring the pressure change in response to the injection of (+) α-TP aggregates into both the Tris and phosphate subphases assessed the influence of the electrolytes on the (+) α-TP nanomaterial interactions with the monolayer. In the presence of Tris the aggregates showed rapid interaction with the monolayer, but in the

ACCEPTED MANUSCRIPT

presence of phosphate there were no interactions between the (+) α-TP nanomaterials and the membrane. These results suggested that the Tris interacted with the membrane to facilitate the nanomaterial membrane interactions whilst phosphate reduced both aggregate and monolayer surface charges, causing an anionic electrostatic repulsive barrier between the aggregate and the monolayer. There is evidence in the literature that large organic monovalent cations, like Tris, can interact with bacterial membranes to make them more permeable [45]-[51] This is thought to be because the ion-pairing can disrupt the phospholipid packing and this can 'sensitise' the membranes to the effects of antimicrobials. This 'sensitisation' can be beneficial in a number of scenarios, for example, Tris has previously been shown to increase the permeability of both nitrocefin and the enzyme lysozyme in the *Pseudomonas aeruginosa* outer membrane [52] and it has also been shown to facilitate stronger interactions of the antibiotic tetracycline with monolayer phospholipids [53].

The magnitude of the POPC: POPG monolayer pressure increase (2.7 mN/ m) when the (+) α-TP nanomaterials were injected into the Tris subphase suggested that the (+) α-TP was inserting into the monolayer rather than rupturing it [54], [55]. This (+) α-TP nanomaterial insertion into the bacterial membrane may account for altered growth of *S. oralis* when compared to (+) α-TP in the presence of phosphate. Although the phosphate buffer was shown to interact with bacterial membranes, that lack of surface pressure increase when (+) α-TP was injected in the presence of the phosphate suggested that it did not alter the membrane permeability [56]. The action of Tris to improve the (+) α-TP interactions with bacterial membranes could improve the bacterial intracellular levels of (+) α-TP. Although (+) α-TP is endogenous in some cells, its intercellular concentrations appears to be highly regulated and increasing its concentration in the cells could be an effective means to trigger cell death as it is a potent signalling molecule that targets enzymes including acid/ alkaline

ACCEPTED MANUSCRIPT

phosphatases, adenosinetriphosphatas, diphosphopyridine nucleotidase and mRNAs encoding enzymes [54], [57]. The differential effects of the (+) α-TP with phosphate and Tris in bacterial growth assays supported the hypothesis that (+) α-TP was more readily taken up by the cells in the presence of Tris. When accompanied by phosphate the bacterial growth assays showed that (+) α-TP has to wait for cell division in order to induce an effect, but in Tris (+) α-TP penetrated the cell to cause an effect immediately upon application.

Using Tris but not phosphate in the dispersion medium allowed the 700 nm (+) α-TP nanostructures to penetrate the salivary biofilms to kill the bacteria in multispecies bacterial communities to greater depths. This data, in light of the aggregate characterisation, Langmuir and planktonic biofilm studies, suggested that the EPS of the oral multispecies biofilm was predominantly negatively charged and this charge was being screened by the positively charged Tris. The EPS has previously been shown to inhibit the diffusion of both positively [58] and negatively [47] charged small organic antimicrobials through electrostatic interaction, but this current work also showed the importance of these electrostatic interactions for comparatively large, 700 nm, aggregates.

Conclusions

The co-administration of anionic (+) α-TP nanomaterials with the cationic electrolyte, Tris, enhanced their penetration into biofilms and their interactions with the bacterial monolayer. This appeared to occur not by diminishing the (+) α-TP nanomaterials negative surface charge, but through diminishing the nanomaterial's electrostatic interactions with the biofilms and the bacterial membranes. These changes facilitating nanomaterial biofilm penetration to enable the bacteria at the heart of the biofilm communities to be killed. Similar effects could not be achieved by the co-administration of the (+) α-TP nanomaterials with the phosphate electrolytes, which provided evidence that it was the screening of negative

ACCEPTED MANUSCRIPT

electrostatic interactions using Tris which produce the beneficial effects. In oral health the tooth surface is an attractive adsorptive site for negatively charged nanomaterials and in our previous work we have found (+) α-TP binds to hydroxyapatite [18]. Hence, the co-administration of Tris with the (+) α-TP nanomaterials to allow penetration to the tooth surface where (+) α-TP could adsorb to the enamel would provide a considerable substantive antimicrobial action.

Funding information

The study was financed by an Engineering and Physical Sciences Research Council (EPSRC) CASE award with Johnson & Johnson Consumer Companies, Inc.

References

[1] Boase, S.; Foreman, A.; Cleland, E.; Tan, L.; Melton-Kreft, R.; Pant, H.; Hu, F. Z.; Ehrlich, G. D.; Wormald, P-J. The Microbiome of Chronic Rhinosinusitis: Culture, Molecular Diagnostics and Biofilm Detection. *BMC Infect. Dis*. **2013**, 13, 210.

[2] Ha, K. R.; Psaltis, A. J.; Butcher, A. R.; Wormald, P. J.; Tan, L. W. In Vitro Activity of Mupirocin on Clinical Isolates of Staphylococcus Aureus and its Potential Implications in Chronic Rhinosinusitis. *Laryngoscope*. **2008**, 118(3), 535–40.

[3] Haagensen, J. A.; Klausen, M.; Ernst, R. K.; Miller, S. I.; Folkesson, A.; Tolker-Nielsen, T.; Molin, S. Differentiation and Distribution of Colistin- and Sodium Dodecyl Sulfate-Tolerant Cells in Pseudomonas. *J Bacteriol*. **2007**, 189(1), 28-37.

[4] Høiby, N.; Bjarnsholt, T.; Givskov, M.; Molin. S.; Ciofu, O. Antibiotic Resistance of Bacterial Biofilms. *Int J Antimicrob Agents*. **2010**, 35(4), 322-32.

ACCEPTED MANUSCRIPT

[5] Zhang, L.; Mah, T-F. Involvement of a Novel Efflux System in Biofilm-Specific Resistance to Antibiotics. *J Bacteriol*. **2008**, 190(13), 4447–4452.

[6] Beaulac, C.; Clement-Major, S.; Hawari, J.; Lagace, J. Eradication of Mucoid Pseudomonas Aeruginosa with Fluid Liposome-Encapsulated Tobramycin in an Animal Model of Chronic Pulmonary Infection. *Antimicrob Agents Chemother*. **1996**, 40, 665–9.

[7] Kim, H. J.; Jones, M. N. The Delivery of Benzyl Penicillin to Staphylococcus Aureus Biofilms by use of Liposomes. *J Liposome Res*. **2004**, 14, 123–39.

[8] Ouyang, L; Deng, Y; Yang, L; Shi, X; Dong, T; Tai, Y; Yang, W; Chen, Z. Graphene-Oxide-Decorated Microporous Polyetheretherketone with Superior Antibacterial Capability and In Vitro Osteogenesis for Orthopedic Implant. Macromol. Biosci. **2018**, 18, 1800036.

[9] Deng, Y; Yang, L; Huang, X; Chen, J; Shi, X; Yang, W; Hong, M; Wang, Y; Dargusch, M. S; Chen, Z. Dual Ag/ZnO-Decorated Micro-/Nanoporous Sulfonated Polyetheretherketone with Superior Antibacterial Capability and Biocompatibility via Layer-by-Layer Self-Assembly Strategy. Macromol. Biosci. **2018**, 18, 1800028.

[10] Li, X; Yeh, Y-C; Giri, K; Mout, R; Landis, R. F; Prakash, Y. S; Rotello, V. M. Control of Nanoparticle Penetration into Biofilms through Surface Design. *Chem Commun (Camb)*. **2015**, 51(2), 282–285.

[11] Saleh, N. B; Chambers, B; Aich, N; Plazas-Tuttle, J; Phung-Ngoc, H. N; Kirisits, M. J. Mechanistic Lessons Learned from Studies of Planktonic Bacteria with Metallic Nanomaterials: Implications for Interactions between Nanomaterials and Biofilm Bacteria. *Front. Microbiol*. **2015**, 6, 677.

[12] Cazander, G; Veerdonk, M.C; Vandenbroucke-Grauls, C. M. J. E; Schreurs, M. W. J; Jukema, G.N. Maggot Excretions Inhibit Biofilm Formation on Biomaterials. Clin Orthop Relat Res. **2010**, 468(10), 2789–2796.

ACCEPTED MANUSCRIPT

[13] Singh, S; Singh, S. K; Chowdhury, I; Singh, R. Understanding the Mechanism of Bacterial Biofilms Resistance to Antimicrobial Agents. *Open Microbiol J*. **2017**, 11, 53–62.

[14] Gupta, A; Landis, R. F; Rotelloa, V. M. Nanoparticle-Based Antimicrobials: Surface Functionality is Critical. *F1000Research*. **2016**, 5(F1000 Faculty Rev), 364.

[15] Wang, L; Hu, C; Shao, L. The Antimicrobial Activity of Nanoparticles: Present Situation and Prospects for the Future. *Int J Nanomedicine*. **2017**, 12, 1227–1249.

[16] Besinis, A; Peralta,T. D; Tredwin,C. J; Handy, R. D. Review of Nanomaterials in Dentistry: Interactions with the Oral Microenvironment, Clinical Applications, Hazards, and Benefits. *ACS Nano*. **2015**, 9(3), 2255-2289.

[17] Lewis, K. Riddle of Biofilm Resistance. *Antimicrob. Agents Chemother*. **2001**, 45(4) 999-1007.

[18] Harper, R. A.; Carpenter, G. H.; Abbate, V.; Proctor, G. B.; Harvey, R. D.; Gambogi, R. J.; Geonnotti, A.; Hider, R.; Jones, S. A. Soft, Adhesive (+) Alpha Tocopherol Phosphate Planar Bilayers that Control Oral Biofilm Growth through a Substantive Antimicrobial Effect. *Nanomedicine*. **2018,** S1549-9634(18)30009-1.

[19] Zhang, Z.; Nadezhina, E.; Wilkinson K. J. Quantifying Diffusion in a Biofilm of Streptococcus mutans. *Antimicrob Agents Chemother*. **2011**, 55(3), 1075–1081.

[20] Golmohamadi, M.; Clark, R. J.; Veinot, J. G. C.; Wilkinson K. J. The Role of Charge on the Diffusion of Solutes and Nanoparticles (Silicon Nanocrystals, nTiO2, nAu) in a Biofilm. *Environ. Chem.* **2013**, 10, 34–41.

[21] Huang, R; Li, M; Gregory, R. L. Bacterial Interactions in Dental Biofilm. *Virulence*, **2011** 2(5), 435–444.

[22] Sutherland, I. W. The Biofilm Matrix: an Immobilized but Dynamic Microbial Environment. *Trends Microbiol*. **2001**, 9, 222–227.

ACCEPTED MANUSCRIPT

[23] Limoli, D. H; Jones, C. J; Wozniak, D. J. Bacterial Extracellular Polysaccharides in Biofilm Formation and Function. *Microbiol Spectr*, **2015**, 3(3).

[24] Larimer, C.; Suter, J. D.; Bonheyo, G.; Addleman, R.S. In Situ Non-Destructive Measurement of Biofilm Thickness and Topology in an Interferometric Optical Microscope. *J Biophotonics*. **2016**, 9(6), 656-66.

[25] Meers, P; Neville, M; Malinin, V; Scotto, A. W; Sardaryan, G; Kurumunda, R; Mackinson, C; James, G; Fisher, S; Perkins, W. R. Biofilm Penetration, Triggered Release and In Vivo Activity of Inhaled Liposomal Amikacin in Chronic Pseudomonas aeruginosa Lung Infections. *J. Antimicrob. Chemother*. **2008**, 61, 859-868.

[26] Liu Y; Busscher H. J; Zhao B; Li Y; Zhang Z; van der Mei H. ;, Ren Y; Shi L. Surface-Adaptive, Antimicrobially Loaded, Micellar Nanocarriers with Enhanced Penetration and Killing Efficiency in Staphylococcal Biofilms. *ACS Nano*. **2016**, 10(4), 4779-89.

[27] Dong, D.; Thomas, N.; Thierry, B.; Vreugde, S.; Prestidge, C. A.; Wormald P-J. Distribution and Inhibition of Liposomes on Staphylococcus aureus and Pseudomonas aeruginosa Biofilm. *PLoS ONE*. **2015**, 10(6), e0131806.

[28] Voss, J. G. Effects of Organic Cations on the Gram-Negative Cell Wall and their Bactericidal Activity with Ethylenediaminetetra-Acetate and Surface Active Agents. *J. gen. Microbiol*. **1967**, 48, 391-400.

[29] Trewby, W.; Livesey, D.; Voïtchovsky, K. Buffering Agents Modify the Hydration Landscape at Charged Interfaces. *Soft Matter*. **2016**, 12, 2642-2651.

[30] Fujiwara, T.; Hoshino, T.; Ooshima, T.; Sobue, S.; Hamada, S. Purification, Characterization and Molecular Analysis of the Gene Encoding Glucosyltransferase from Streptococcus oralis. *Infect Immun.* **2000**, 68, 2475–2483.

[31] Cavalcanti, I.M.G.; Del Bel Cury, A.A.; Jenkinson, H.F.; Nobbs, A.H. Interactions between Streptococcus oralis, Actinomyces oris, and Candida albicans in the Development of

ACCEPTED MANUSCRIPT

Multispecies Oral Microbial Biofilms on Salivary Pellicle. *Molecular Oral Microbiology*. **2017**, 32, 60–73.

[32] Chenga, J. T. J.; Haleb, J. D.; Elliott, M.; Hancock, R. E. W.; Strausa, S. K. The Importance of Bacterial Membrane Composition in the Structure and Function of Aurein 2.2 and Selected Variants. *BBA – Biomembranes.* **2011**, 1808(3), 622–633.

[33] Negis, Y., Meydani, M., Zingg, J.M., and Azzi, A. Molecular Mechanism of Alpha-Tocopheryl-Phosphate Transport Across the Cell Membrane. *Biochem Biophys Res Commun*. **2007**, 359(2), 348-53.

[34] Erbe, A.; Kerth, A.; Dathe, M.; Blume, A. Interactions of KLA Amphipathic Model Peptides with Lipid Monolayers. *ChemBioChem*. **2009**, 10(18), 2884–2892.

[35] Dalgaard, P.; Koutsoumanis, K. Comparison of Maximum Specific Growth Rates and Lag Times Estimated from Absorbance and Viable Count Data by Different Mathematical Models. *J. Microbiol. Methods.* **2001**, 43, 183 – 196.

[36] Zeng, J.; and Chong, P. L-G. Effect of Ethanol-induced Lipid Interdigitation on the Membrane Solubility of Prodan, Acdan, and Laurdan. *Biophys J*. **1995**, 68, 567-573.

[37] Langner, M.; Pruchnik, H.; Kubica, K. The Effect of the Lipid Bilayer State on Fluorescence Intensity of Fluorescein-PE in a Saturated Lipid Bilayer. *Z. Naturforsch*. **2000**, 55c, 418-424.

[38] Cugia, F.; Monduzzi, M.; Ninham, B. W.; Salis, A. Interplay of Ion Specificity, pH and Buffers: Insights from Electrophoretic Mobility and pH Measurements of Lysozyme Solutions. *RSC Adv*. **2013**, 3, 5882-5888.

[39] Guerrero-Garcıa, G. I.; Gonzalez-Tovar, E.; de la Cruz, M. O. Effects of the Ionic Size-Asymmetry around a Charged Nanoparticle: Unequal Charge Neutralization and Electrostatic Screening. *Soft Matter*. **2010**, 6, 2056–2065.

[40] Chou, T. H.; Chang, C. H. Thermodynamic Characteristics of Mixed DPPC/DHDP

ACCEPTED MANUSCRIPT

Monolayers on Water and Phosphate Buffer Subphases. *Langmuir 2000*. **2000**, 16, 3385-3390.

[41] Nowotarska, S. W.; Nowotarski, K. J.; Friedman, M.; Situ, C. Effect of Structure on the Interactions between Five Natural Antimicrobial Compounds and Phospholipids of Bacterial Cell Membrane on Model Monolayers. *Molecules*. **2014**, 19, 7497-7515.

[42] Petrache, H. I; Trizma® tram-Nagle, S; Harries, D; Kučerka, N; Nagle, J. F; Parsegian V. A. Swelling of Phospholipids by Monovalent Salt. *J Lipid Res*. **2006**, 47(2), 302–309.

[43] Negi, S.; Futami, E.; Tsukube, H.; Kano, K. Effects of Anions in Subphases on a Langmuir Monolayer of N,N-Dimethyl-1-octadecanamine. *Bull. Chem. Soc. Jap.* **2000**, 73(4), 977-984.

[44] Kahn, J. G.; Monroy, F.; Mingotaud. C. Adsorption of Large Inorganic Polyanions under a Charged Langmuir Monolayer: an Ellipsometric Study. *Phys. Chem. Chem. Phys*. **2003**, 5, 2648-2652.

[45] Hamouda, T.; Baker (Jr), J. R. Antimicrobial Mechanism of Action of Surfactant Lipid Preparations in Enteric Gram-Negative Bacilli. *J. Appl. Microbiol*. **2000**, 89(3), 397–403.

[46] Irvin, R. T.; Macalister, T. J.; and Costerton, J. W. Trizma® (hydroxymethyl)aminomethane Buffer Modification of Escherichia coli Outer Membrane Permeability. *J. Bacteriol*. **1981**, 145(3), 1397-1403.

[47] Ban, S. H.; Kim, J. E.; Pandit, S.; Jeon, J. G. Influences of Dryopteris Crassirhizoma Extract on the Viability, Growth and Virulence Properties of Streptococcus mutans. *Molecules*. **2012**, 17, 9231-9244.

[48] Asbell, M. A.; Eagon, R. G. Role of Multivalent Cations in the Organization, Structure, and Assembly of the Cell Wall of Pseudomonas aeruginosa. *J Bacteriol*. **1966**, 92(2), 380-387.

ACCEPTED MANUSCRIPT

[49] Vaara, M. Agents that Increase the Permeability of the Outer Membrane. *Microbiol Rev*. **1992**, 56(3), 395-411.

[50] Lambert, P. A. Cellular Impermeability and Uptake of Biocides and Antibiotics in Gram-Positive Bacteria and Mycobacteria. *J. Appl. Microbiol*. **2002**, 92(s1), 46S–54S.

[51] Tris amino technical data sheet-Angus chemical company. Available online at [https://webcache.googleusercontent.com/search?q=cache:Z8nuSYDb_MkJ:https://www.angus.com/literature/downloaddoc%3FfileName%3DANGUS_LifeSciences_TRISAMINO_TDS.pdf%26contentType%3DTechnical%2520Data%2520Sheet%26parentFolder%3DLiterature+&cd=3&hl=en&ct=clnk&gl=uk] accessed **12/Aug/2016**.

[52] Hancock, R. E. W.; Wong, P. G. W. Compounds which Increase the Permeability of the Pseudomonas aeruginosa Outer Membrane. *Antimicrob. Agents Chemother*. **1984**, 26(1), 48-52.

[53] Mecheri, B.; Gambinossia, F.; Nocentinib, M.; Puggellia, M.; Caminati, G. Modulation of Tetracycline–Phospholipid Interactions by Tuning of pH at the Water–Air Interface. *Biophys. Chem*. **2004**, 111(1), 15–26.

[54] Posada, I. M. D.; Busto, J. V.; Goñi, F. M.; and Alonso, A. Membrane Binding and Insertion of the Predicted Transmembrane Domain of Human Scramblase 1. *BBA – Biomembranes*. **2014**. 1838(1) Part B, 388–397.

[55] Wang, B. Y.; Hong, J.; Ciancio, S. G.; Zhao, T.; Doyle, M. P. A Novel Formulation Effective in Killing Oral Biofilm Bacteria. *J Int Acad Periodontol*. **2012**, 14(3), 56-61.

[56] Schwab, U.; Gilligan, P.; Jaynes, J.; Henke, D. In Vitro Activities of Designed Antimicrobial Peptides against Multidrug-Resistant Cystic Fibrosis Pathogens. *Antimicrob. Agents Chemother*. **1999**, 43(6), 1435-1440.

[57] Zingg, J. M.; Meydani, M.; Azzi, A. α-Tocopheryl Phosphate – An Active Lipid Mediator? *Mol. Nutr. Food Res.* **2010**, 54, 679–692.

ACCEPTED MANUSCRIPT

[58] Shen, Y.; Zhao, J.; Fuente-Núñez, C.; Wang, Z.; Hancock, R. E. W.; Roberts, C. R.; Ma, J.; Li, J.; Haapasalo, M.; Wang, Q. Experimental and Theoretical Investigation of Multispecies Oral Biofilm Resistance to Chlorhexidine Treatment. *Sci. Rep*. **2016**, 6, 27537.

ACCEPTED MANUSCRIPT